Liquid crystal phase of counter-rotating staircases – A case of antiferrochirality

Ya-xin Li
Xi'an Jiaotong University https://orcid.org/0000-0001-8221-8035
Hong-fei Gao
Yunnan University
Rui-bin Zhang
University of Sheffield
Kutlwano Gabana
University of Sheffield
Qing Chang
Yunnan University
Gillian Gehring
University of Sheffield
Xiao-hong Cheng
Yunnan University
Xiangbing Zeng
University of Sheffield
Goran Ungar (g.ungar@sheffield.ac.uk)
Xi'an Jiaotong University https://orcid.org/0000-0002-9743-2656

Article

Keywords: liquid crystals (LC), helical structures

Posted Date: April 9th, 2021

DOI: https://doi.org/10.21203/rs.3.rs-256979/v1

Liquid crystal phase of counter-rotating staircases – A case of antiferrochirality

Ya-xin Li[1,2], Hong-fei Gao[3], Rui-bin Zhang[2], Kutlwano Gabana[4], Qing Chang[3], Gillian A. Gehring[4], Xiao-hong Cheng[3,5]*, Xiang-bing Zeng[2]* and Goran Ungar[1,2]*

1. State Key Laboratory for Mechanical Behaviour of Materials, Shaanxi International Research Centre for Soft Matter, Xi'an Jiaotong University, Xi'an, 710049, P. R. China. Email: g.ungar@xjtu.edu.cn; g.ungar@sheffield.ac.uk
2. Department of Materials Science and Engineering, University of Sheffield, Sheffield S1 3JD, UK. E-mail: x.zeng@sheffield.ac.uk
3. Key Laboratory of Medicinal Chemistry from Natural Resources, Ministry of Education, Yunnan University, Kunming, P. R. China
4. Department of Physics and Astronomy, University of Sheffield, Sheffield E1 2C, UK
5. School of Chemistry and Chemical Engineering, Yangtze Normal University, Fuling, P. R. China. E-mail: xhcheng@ynu.edu.cn

Abstract

Helical structures continue to inspire, and there is considerable temptation to attribute helicity to columnar liquid crystals (LC). While short isohelical sequences are undoubtedly present, and longer ones in chiral or chiral-doped compounds, the order is only short-range, equivalent to a paramagnet without or with field. However, here we report a confirmed example of a true LC phase of achiral compounds consisting of columns, each being a long-range homochiral helix. Long-range periodicity and isochirality are maintained by intercolumnar interaction. This orthorhombic LC, spacegroup *Fddd*, is discovered in compounds with either bent or straight rod-like pi-conjugated cores. There are 4 right and 4 left-handed ribbons or star-profiled columns per unit cell. The structure is equivalent to an antiferromagnet with twist replacing spins. A theory based on interacting quadrupoles confirms this structure as energetically favoured over alternatives. The findings open a new approach to homochirality in achiral compounds, with promising optical/chiroptical properties.

Columnar liquid crystal (LC) phases, most often of hexagonal 2D symmetry (Col_{hex}), are best known in compounds with disc- and

wedge-shaped molecules[1,2,3,4,5,6,7], in honeycomb-forming rod-like amphiphiles with side-chains[8,9,10], and in "polycatenar" rod-like molecules with more than one chain at each end[11,12]. There are a number of claims of helical columnar LCs of achiral compounds[13], some of them ingeniously designed with high barrier to conformational flip (e.g. "propeller-blade" bipyridines[14]). The claims are often based on layer-lines observed in fibre X-ray patterns, but their long-range isochirality has not been proven convincingly, because layer-lines are just as likely in fibre patterns of completely random-walk chains[15]. In the extreme, placing a brick rotated on top of another creates a portion of a helix. Even when the molecules have a chiral group with enantiomeric excess (ee) or a chiral dopant is added, while there is amplified preponderance of one helical hand ("sergeants-and-soldiers"), the length of homochiral sequences is limited and ee-dependent. This short-range order is characteristic of a paramagnet, with ee or dopant acting as external field. However, the question requiring answer is whether twist sense can propagate to true long range in columns of true LCs, including those of achiral compounds. Can column helicity be of ferromagnetic type? Can we have examples of ferrochirality[16] or even antiferrochirality?

Polycatenars also show bicontinuous cubic (Cub_{bi}) phases[12,17,18]. Recently it was discovered that the 3D networks in Cub_{bi}[19,20] and related polycatenar mesophases[21] consist of twisted ribbon-like segments, inducing chirality in non-chiral compounds and propagating single hand to macro-scale via homochiral network junctions.[14,17,21] In the absence of such defect-correcting junctions, columnar LCs of similar compounds are thought to contain twist but are unable to sustain long-range helical sense as helix reversals cannot be prevented in an isolated 1D column. In contrast, in column-containing crystals helical sense propagates as reversals are inhibited by interactions with "correctly" positioned molecules on surrounding lattice; prime examples are various soft-crystal forms of dendronized perylene bisimides (PBIs)[22], different "ordered" discotic phases[23] or in numerous achiral crystalline synthetic polymers. Many helical soft crystals transform to Col_{hex} at higher temperatures, e.g. PBIs and some polymers such as Teflon. Teflon's chains lose their regular helicity on transition from crystal to columnar LC at 30°C[24,25], probably with soliton-like helix reversals[26].

Here we report a new 3D LC phase where we show conclusively that homochirality of helical columns can indeed propagate to long-range even without molecular chirality or network junctions. The phase consists of counter-rotating twisted columns with el-

liptical or star-like cross-section. There is long-range order between helical columns but *not* between molecules, hence it is a liquid crystal and not a crystal. Two of the compounds involved contain a chromophore, with the helical configuration enabling efficient π-π stacking, making them interesting for opto-electronic applications. A simple theory based on interacting quadrupoles is developed, confirming that, compared to the alternatives, the observed structure is energetically the optimal packing of helices of linear polycatenar dumbbells.

The materials

The new *Fddd* phase is found in two types of polycatenars with three chains at each end, one with straight (**FCN16** and **FO16**) and the other with bent core (**IC^3/n** – see Table 1). The synthesis of **IC^3/n** compounds has been reported previously[27], while that of **FCN16**/**FO16** is described in Methods and in Section S10, Supplementary Information (SI).

Table 1 Phase transition temperatures on cooling.

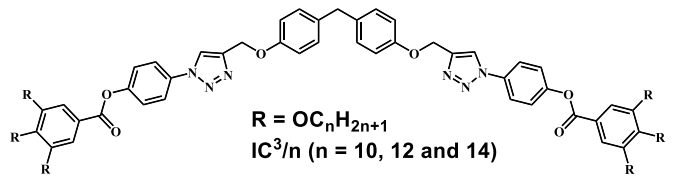

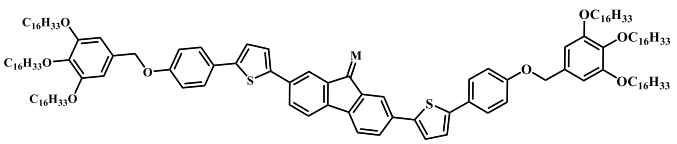

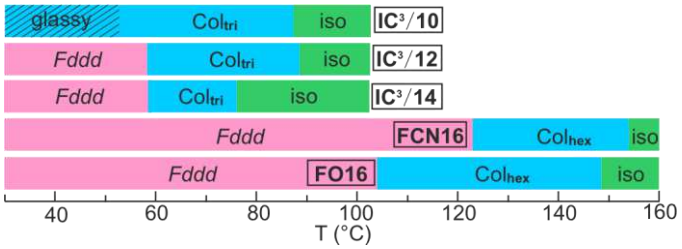

Name	*Lattice parameters* (Å)[a]	*n*[b]	*T*/°C [Δ*H*/J g^{-1}][c]
IC^3/10	a_{tri} = 48.9	3	Iso 87.4 [0.7] Col$_h$ 52.8 [7.1] glassy
IC^3/12	a_{tri} = 51.3	3	Iso 88.6 [0.4] Col$_h$ 58.3 [6.2] ***Fddd***
	a_{orth}=173.5 b_{orth}=106.1 c_{orth}=40.8	3	
IC^3/14	a_{tri} = 52.8	3	Iso 76.2 [0.1] Col$_h$ 58.5 [7.2] ***Fddd***
	a_{orth}=186.8 b_{orth}=107.8 c_{orth}=40.8	3	
FCN16	a_{hex}=54.1	3	Iso 154.4 [0.8] Col$_h$ 123.2 [17.0] ***Fddd*** 27.9 [46.9] Cr
	a_{orth}=186.9 b_{orth}=107.9 c_{orth}=34.9	2	
FO16	a_{hex}=53.9	3	Iso 148.3 [0.3] Col$_h$ 103.8 [3.9] ***Fddd*** 29.0 [9.7] Cr
	a_{orth}=186.0 b_{orth}=107.4 c_{orth}=32.5	2	

a: Lattice parameters of hexagonal and trigonal columnar phase a_{hex} and a_{tri}, and orthorhombic *Fddd* phase a_{orth}, b_{orth} and c_{orth}.

b: Number of molecules per column stratum in columnar and *Fddd* phases (see Table S8, footnotes d-g).

c: Peak DSC transition temperatures [enthalpies] at 5 K min^{-1} for IC^3/n and 10 K min^{-1} for FCN16 and FO16. Cr = crystal, Col$_{tri}$ /Col$_{hex}$ = trigonal/hexagonal columnar, Iso = isotropic melt. For more DSC data see Fig. S1.

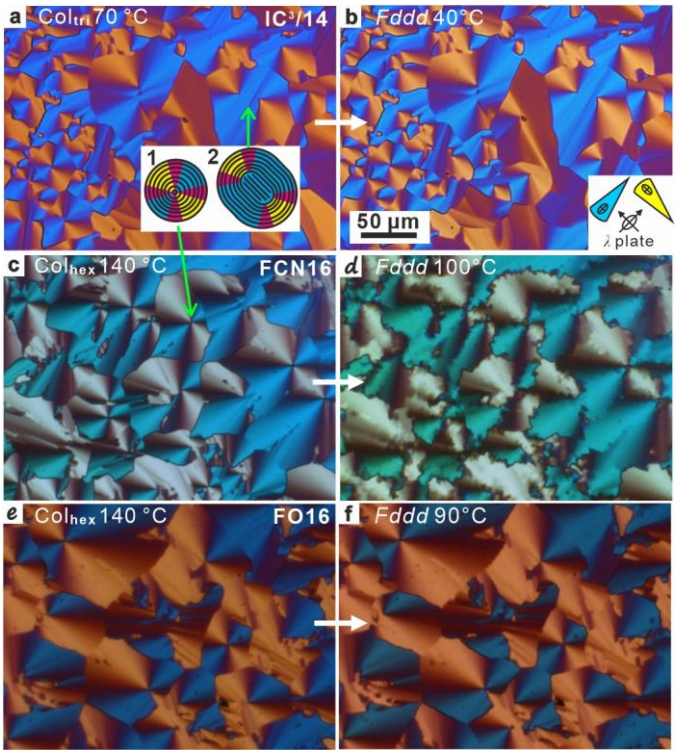

Fig. 1 Polarized optical micrographs. a,c,e, columnar and **b,d,f,** *Fddd* phases of compounds (**a**, **b**) IC^3/14, (**c**, **d**) FCN16 and (**e**, **f**) FO16. Recorded with a full-wave (λ) plate. Inset in **a** depicts two developable domains with (1) a s=+1 disclination and (2) two +½ disclinations, the latter indicating stiffer columns; black lines are column trajectories. Inset in **b** shows orientation of indicatrices of λ-plate and coloured fans. See more textures in Section S2, SI.

All compounds form a uniaxial columnar phase at higher temperatures, **IC^3/n** one with trigonal (Col$_{tri}$)[27], and **FCN16** and **FO16** one with hexagonal symmetry (Col$_{hex}$), see Table 1 and Figs. 2a,e,f, S1, S7, S8, S10, S11. Both phases are also referred to collectively as Col. Below Col all except **IC^3/10** also form a 3D LC phase, the focus of this study. Its structure is determined by detailed X-ray study and by atomic force microscopy (AFM), see next section. Fan ("spherulitic") textures, typical of columnar developable domains[28], appear in polarized optical micrographs (POM, Figs. 1, S2-S4). Comparing insets in Fig. 1**a** and **b** we see that the slow axis, hence the aromatic cores, is roughly perpendicular to column axis. The increase in birefringence on phase transition is most pronounced in **FCN16** (Fig. 1c,d) where, from Michel-Levy colour chart, optical retardation increases by 1/3 (from ~150 to ~200 nm), indicating molecular alignment closer to column normal in the low-T phase.

Structure of the new mesophase

The absence of second harmonic (SHG) in the high-T phase of **FCN16**/**FO16** means that the hexagonal Laue symmetry of the small-angle X-ray (SAXS) pattern (Figs. 2f, S8, S11) comes from a Col_{hex} phase, unlike in **IC^3/n** where the presence of SHG indicates trigonal symmetry[27]. As in the Col phase, only a diffuse wide-angle X-ray scattering (WAXS) maximum at 4.5Å (q=1.40Å^{-1}) is observed for **IC^3/n** in the low-T phase (Fig. S5b). This confirms the LC nature of the phase. An additional narrower but still diffuse peak appears at 3.4Å (1.85Å^{-1}) in the low-T phase of **FCN16** and **FO16** (Figs. 2e, S7, S10). Its near-meridional position as a vertical streak close to the horizon in the grazing incidence (GIWAXS) pattern of a sheared film (Figs. 2g-j) identifies it as arising from good π-π stacking along z (column) axis of parallel aromatic planes.

The transmission powder SAXS patterns of low-T phase of the compounds are rather complex (Figs. 2a, S6a, S12a). The observed diffraction peaks can be indexed to an orthorhombic lattice (a~180Å, b ~110Å and c ~40Å, Table 1) with the help of grazing incidence SAXS (GISAXS) on surface-oriented thin films (IC^3/12, Fig.2b; IC^3/14, Fig. S6b; FCN16, Figs. 2c, S9; FO16, Fig. S12b). The GISAXS patterns confirm the reflection conditions h+k, h+l, k+l even, and h+l, h+k equal to 4n for h0l and hk0. This narrows the choice of spacegroup to *F*2*dd* or *Fddd* (Table S2). As no 0kl reflection was observed, the deciding condition k+l=4n could not be tested hence, as usual in LCs, the higher symmetry *Fddd* is adopted.

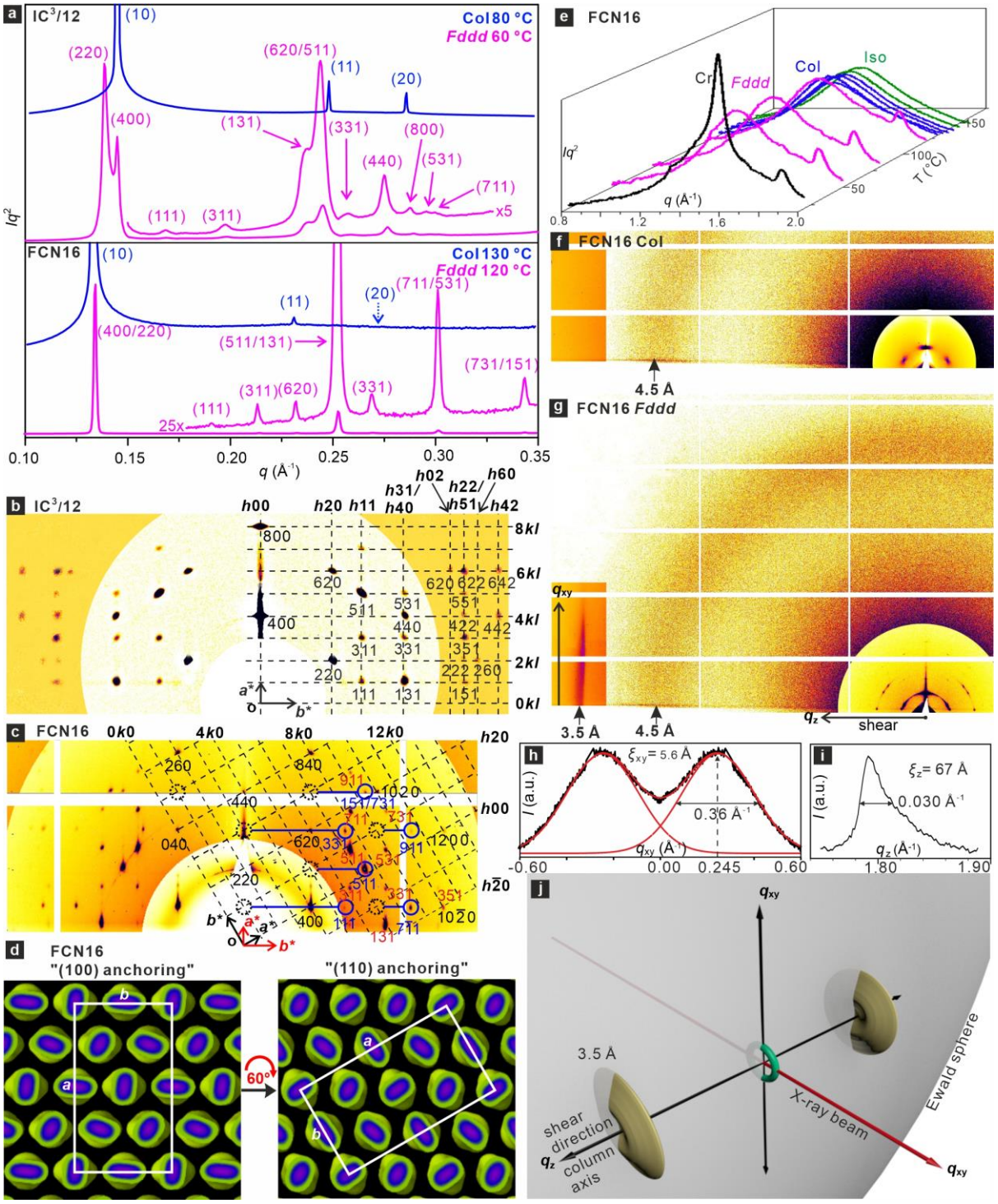

Fig.2 X-ray diffraction results. a, Transmission powder SAXS curves of Col and *Fddd* phases of **IC^3/12** and **FCN16**. **b**,**c,** GISAXS patterns of *Fddd* phase of **IC^3/12** and **FCN16**. Background was subtracted and the higher-*q* zone is intensity-enhanced. Partial reciprocal *hk*0 lattice plane is superimposed, with some *hkl* spots in **c** circled blue and connected to their *hk*0 base by blue row lines (for calculation see Fig. S9). Reflections in **c** come from two orientations with (110) and (100) planes anchored on Si substrate; reflections in red are from the latter. **d**, Real space **FCN16**: in both orientations the LC faces substrate with a dense plane of columns (unit cell in white). **e**, Evolution of powder WAXS of

FCN16 on heating. **f,g**, GIWAXS of lightly sheared film of **FCN16** in Col (130°C) and *Fddd* (100°C) phases, respectively; note the absence of the 3.5Å streak in Col. **h**,**i**, q_{xy} (vertical) and q_z (horizontal) scans of the 3.5Å streak in **g**; in **h** the peak is reflected across the horizon to facilitate curve resolution. **j**, Reciprocal space description of diffraction geometry in **g**, showing symbolically a SAXS ring and the 3.5Å disks.

Electron density (ED) maps were reconstructed from SAXS intensities (Section S4, SI)). According to the map of the low-T phase of **IC^3/12** (Fig. 3a,c) there are eight columns in the unit cell. As in the Col phase[27], the calculated number of molecules in each column stratum of thickness 4.5Å is 3 (Tables 1 and S8). The cross-section of columns is rounded triangular, similar to that in the Col phase, three bent-core molecules back-to-back forming a three-arm star[27]. However, in contrast to the high-T phase, the orientation of the stars changes monotonically with increasing *z*-elevation, resulting in four left- and four right-handed helical "staircases". Assuming uniform twist, each consecutive three-arm stratum, or step, is rotated by 13.3° around the column axis – see model in Fig. 3b,d. A molecular model of a layer with periodic boundary conditions, using the experimental lattice constants and subjected to 30 cycles of molecular dynamics (MD) annealing is shown in Fig. 4c; note efficient space-filling.

The ED map of the *Fddd* phase of **FCN16** (Fig. 3e,g) shows even more clearly the twist of the columns, here appearing like twisted ribbons[29]. The column section is now oval, with close to two parallel linear molecules per column stratum, referred to below as "dimer" (Tables 1 and S8); see also Fig. 3f and the MD snapshot in Fig. 4d. Even though the strata are thinner than in **IC^3/n** (3.4-3.5Å), the twist between strata in the linear compounds is larger (18°), making the pitch (=2*c*) considerably shorter – compare models in Figs. 3d,h.

All columns in (100) rows along *b*-axis co-rotate, either clockwise or anticlockwise, but along {110} diagonals they counter-rotate, alternating between left and right helicity (Fig. 3a-h). *xy* sections of the model at different *z*-elevations (Fig. 4a,b and S15-16) show that the linear dimers of **FO16** and **FCN16** succeed in evading clashes at every level, while the co-rotating stars of **IC^3/n** unavoidably clash along *b* at *z*=4.5Å and *z*=13.5Å. Interestingly, while the *a/b* ratio for **FCN16**, **FO16** and **IC^3/14** is exactly $\sqrt{3}$ (186.9/107.9, 186.0/107.4, 186.8/107.8), meaning that the column axes sit precisely on a hexagonal lattice, for **IC^3/12** the ratio is 1.635, i.e. the unit cell is stretched along the clash direction *b* (Fig. 4a). The deviation from hexagonal grid also causes separa-

tion of (400) and (220) reflections (Figs. 2a). Probably the “padding” by the C12-chains is insufficient to fully mitigate the clashes. Significantly, **IC^3/10** does not form *Fddd* at any temperature (Table 1).

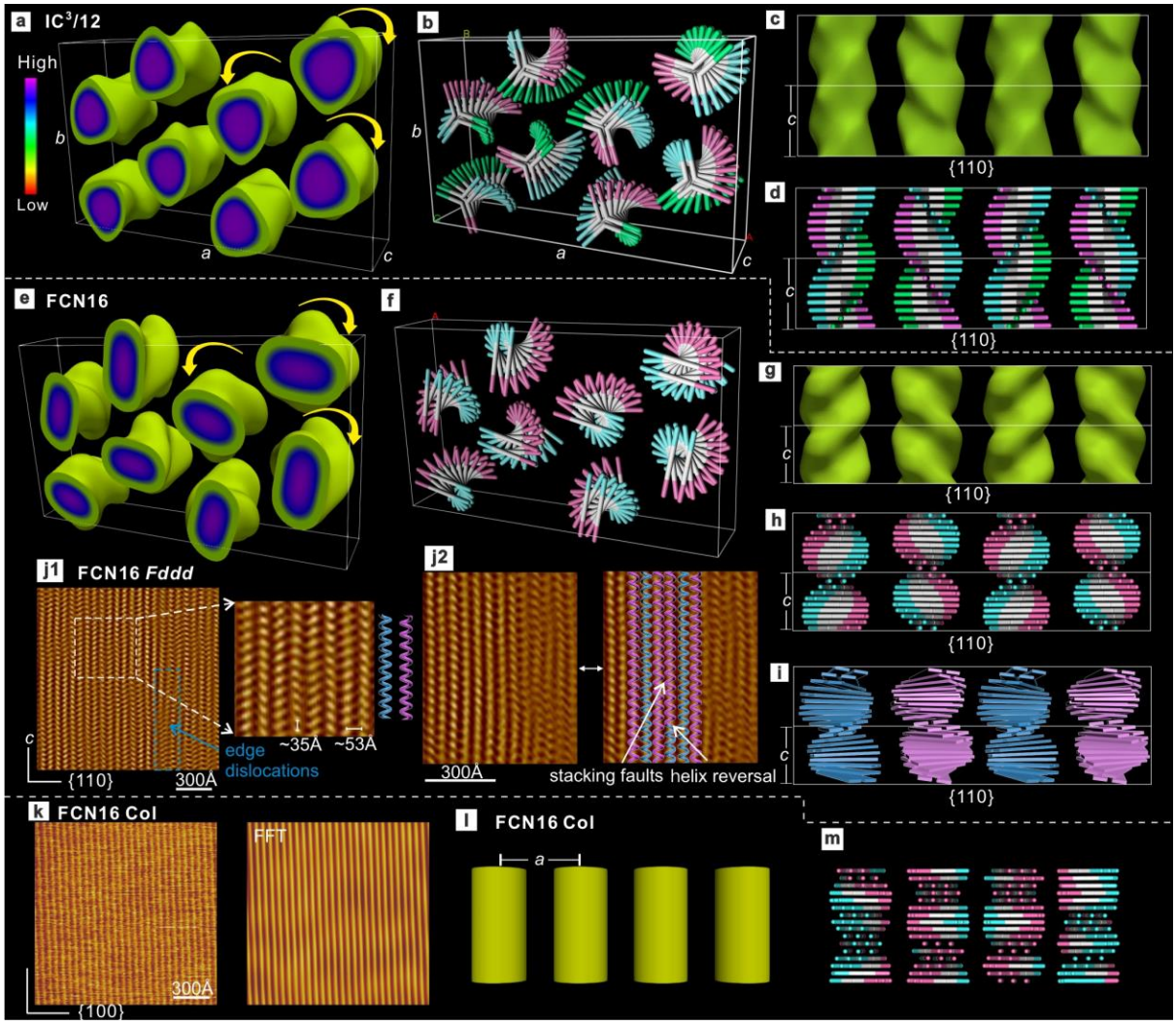

Fig. 3 ED maps, schematic models and AFM images. ED maps and stylized models of *Fddd* phase of **(a-d) IC^3/12** and (**e-h**) **FCN16,** and (**l,m**) of the Col phase of **FCN16**. **(a,c,e,g**) 3D maps with high ED regions (aromatic) enclosed within isoelectron surface (see also supporting videos). (**b,d,f,h),** Schematic models of winding rod-like molecular cores (“staircases”. The two or three core end-groups are coloured differently for clarity. The high positional order is grossly exaggerated. **c,d,g,h**, View along *b*-axis. **i**. A more realistic model of **h** taking account of the 8° molecular tilt. **j**, AFM of *Fddd* phase of FCN16 recorded at 50 °C (Fourier-filtered height image). The enlarged area shows alternating left- and right-handed columns; stacking faults of mismatched chirality and a helix reversal are indicated in (**j2)**. **k**, original AFM image and inverse FFT of Col phase of **FCN16**. **l**, ED map (time/space average by SAXS) and **m,** random twist model (an instantaneous arrangement) of Col phase of **FCN16**.

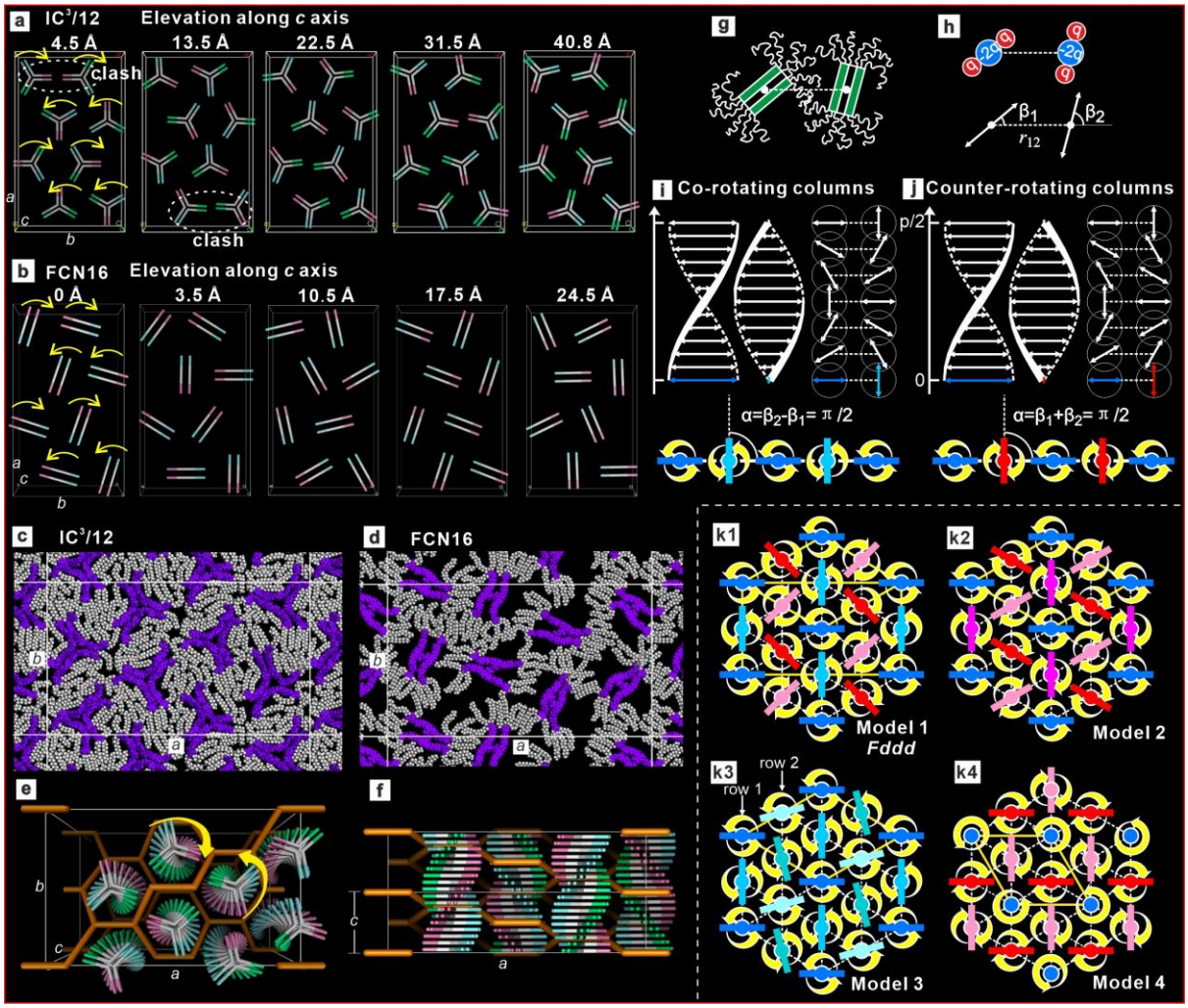

Fig. 4 Models of *Fddd* and its alternatives. a,**b**, Layers at different *z*-elevation for (**a**) **IC^3/n** and **(b**) **FCN16**/**FO16**. **c**,**d**, Snapshots of MD-annealed atomistic models (*xy* layer; purple: aromatic, grey/white: aliphatic). **e,f,** Comparison of network model of *Fddd* phase in poly(styrene-*b*-isoprene) (yellow rods) with model of **IC^3/n**. Arrows indicate helical sense of both columns and network. **g**,**h**, Two dimers of **FO16**/**FCN16** on neighbouring columns in **g** represented by quadrupoles in **h**, where geometrical parameters are also defined. **i**,**j**, Side and top views of (**i**) co-rotating and **(j**) counter-rotating ribbons. **k**. Minimum energy configurations on a 2D hexagonal lattice; (**k1**) two left- and two right-handed columns in a 2x2 supercell, equivalent to the *Fddd* structure here observed experimentally; (**k2**) three left- and one right-handed column in a 2x2 supercell; (**k3**) four right-handed columns in a 2x2 supercell; it turns out that vertical shifting of the second row of columns relative to the first does not change the system energy (**k4**) two left- and one right-handed column in a $\sqrt{3} \times \sqrt{3}$ supercell. The orientation of right-handed columns can be random, which does not affect the system energy (*cf.* structure in ref. 23). In (**k1**-**k4**) right-(left-)handed columns are shades of blue (red).

The alternating helices in *Fddd* phase are also observed directly by AFM on **FCN16** (Figs. 3j, S18, S19). Columns without helicity

are observed in the Col phase in Fig. 3k, matching the ED map and model in Figs. 3l,m. The ~53Å distance between helical columns in Fig. 3j and the ~35Å helical pitch match almost exactly the ED map and the proposed structural model of *Fddd*. Edge dislocations, stacking faults of mismatched chiral columns and helix reversal defects are also seen in Fig. 3j.

An interesting consequence of the different column cross-sections in **IC^3/n** and **FCN16**/**FO16** appears to be a higher bending modulus of the star-like **IC^3/n** columns compared with that of the bendable ribbons of **FCN16**/**FO16**. The difference is evident in the type of disclinations in POM images in Fig. 1; only **FCN16**/**FO16** columns can tolerate the high curvature at the centre of a *s*=+1 disclination (Fig. 1a, inset 1), while the stiffer **IC^3/n** columns prefer ends to sharp bends.

3D order of helices, not molecules

The high surface alignment in GISAXS/GIWAXS experiments allows some further structure refinement and clarification of the true nature of the mesophase. Significantly, the 3.4Å peak in powder WAXS (Fig. 2e) corresponds to the streak at q_z=2π/3.5Å in GIWAXS of columns aligned parallel to substrate (Figs. 2g, S13b). The 0.1Å difference comes from the 8° tilt of the aromatic planes from the *xy* plane, causing a displacement of the intensity maximum away from the *z*-axis (horizon); see $I(q_{xy})$ intensity profile, Fig. 2h. The tilt is taken into account in the model in Fig. 3i, which is more realistic than the simplified version in 3h.

Notably, while there are many small-angle Bragg reflections with resolution-limited width, i.e. with correlation lengths of ca 1800Å (domain size >5000Å), there are no Bragg reflections at wide angles. This means that *Fddd* is a true LC and not a crystal. A more precise distinction is provided by the 3.5Å streak. From the q_z-profile the correlation length along the columns is $\xi_z = 2/\Delta q_z$ = 67 Å (Fig. 2i). However, from the q_{xy}-profile along the streak we get $\xi_{xy} = 2/\Delta q_{xy}$ = 5.6 Å, or "crystal size" of $\pi\xi_{xy}$ = 18 Å, which is smaller even than the width of one single column (>50 Å). These measurements confirm decisively that the *Fddd* is a true LC and *not* a crystal, soft or otherwise, as in many reported helical column-like soft structures. Thus, while there is true 3D long-range order in packing of helical columns, there is no intercolumnar correlation between positions of individual molecules. One may think of the *Fddd* phase as consisting of orderly interlocked helical tubes filled with mobile molecules with no preferred position and no lattice. A somewhat similar situation has been observed previously in a chiral helicene, but with substantially lower order in "tube" packing[30].

Antiferrochirality

Spontaneous long-range alignment modes of electric dipoles in SmC* LCs (layers of tilted chiral molecules) and in some bent-rod LCs, are well known, respectively, as ferroelectric or antiferroelectric[31]. In the same vein it is useful to regard the present *Fddd* phase as "antiferrochiral". This helps distinguishing it from the reported cases of helical columns, where the range of homochirality is short and dependent on the possible presence of chiral substituents or dopants, which act as external field acts on a paramagnet. The well-known frustration of antiferromagnets on a triangular lattice is also present here, causing symmetry-breaking to orthorhombic.

Comparison with cubic LCs and *Fddd*-phase in block copolymers

A phase with *Fddd* symmetry, albeit with a distinctly different structure, has been reported previously in block copolymers (BCPs)[32,33]. The *Fddd* lattice parameters[34] in poly(styrene-*b*-isoprene) or poly(isoprene-*b*-styrene-*b*-ethyleneoxide) are naturally an order of magnitude larger, *a* varying from 750 to 2125 Å[35] . However, the *a*:*b* ratio is similar to that in our LCs, about $\sqrt{3}$:1 (Table S9). Unlike our LC phase which consists of columns, the *Fddd* in BCPs is a single network bicontinuous phase with 3-way junctions, as shown in orange, scaled, in Fig. 4e,f together with our **IC^3/12** model. In *Fddd* phase of PS-*b*-PI, PS forms the network embedded in PI[34]. In a crude analogy, the aromatic cores in our model can be said to occupy PI-rich areas in the BCP phase. Evidently the **IC^3/n** helical columns fill the space between network segments, with the twist sense of the columns matching that of the surrounding network. The *Fddd* phase in BCPs is found between lamellar and Cub$_{bi}$ phases ($Ia\bar{3}d$ or $I4_132$)[32], while our *Fddd* appears below the columnar.

The chiral columns in *Fddd* phase remind us of helical segments of networks forming the double-gyroid cubic $Ia\bar{3}d$ phase[17], the triple-network cubic $I23$[20] or the tetragonal "Smectic-Q" ($I4_122$)[21]. While the latter two are chiral even in achiral compounds, the two networks in the $Ia\bar{3}d$ have opposite hands, resulting in no overall chirality. In all three phases the twist between successive molecular strata is 8-10°. As in the *Fddd*, this twist balances the tendencies for the conjugated rod-like cores to be parallel, maximizing their π-overlap, and that for steric repulsion of the end-chains. Since the compounds forming the above bicontinuous phases contain only 3-4 end-chains, their smaller twist than the ~18° in the 6-chain **FCN16**/**FO16** is understandable.

In bicontinuous phases the homochirality of each network is enforced at junctions, where all three or four merging helical segments must be homochiral to minimize steric clash. However in the *Fddd* there are no junctions and the columns are parallel. What propagates their homochirality is the 3D order of interlocking helices which ensures that helix reversals, such as that in Fig. 3j2, are eventually corrected by the surrounding lattice. In columnar phases of covalent or self-assembled discs columns have cylindrical symmetry, hence such 3D interlock is unlikely. The present results thus suggest that a noncircular column cross-section, such as oval or star-like, is beneficial in facilitating 3D interlock that could sustain homochirality.

A simple theory of packing of helices: *Fddd* and alternative models

The interaction between two **FCN16**/**FO16** dimers from neighbouring columns at the same elevation can be described quantitatively as that between two linear quadrupoles oriented at β_1 and β_2 (Fig. 4g,h). Considering each helix as a series of such twisting quadrupoles, the interaction energy *E* between two neighbouring columns is the sum of interactions between their corresponding quadrupoles at all elevations. Our calculations (Section S9) show that *E* is determined by constant α, defined as $\alpha = \beta_2 - \beta_1$ for co-rotating and $\alpha = \beta_1 + \beta_2$ for counter-rotating columns (Fig. 4i,j).

For a row of columns the minimum *E*, E_{min}, is found for counter-rotating columns with $\alpha = \beta_1 + \beta_2 = \pi/2$ (Fig. 4j). If all columns must co-rotate, a higher E_{min} has $\alpha = \beta_2 - \beta_1 = \pi/2$ (Fig. 4i). In $\frac{3\phi^2}{32r_{12}^5}$ units, where ϕ is the quadrupole moment and r_{12} the distance between quadrupoles, E_{min} per dimer/quadrupole is -29 in a counter-rotating, 3 in a co-rotating, and 6 in a random row. However, the condition to keep all neighbouring columns counter-rotating cannot be satisfied on a 2D-hexagonal lattice. The obvious choice then is to keep as many counter-rotating neighbours as possible, as shown in Fig. 4k1. A 2x2 supercell is assumed, as both counter- and co-rotating minimum-energy rows have a two-column repeat (Fig. 4i,j). We have two left- and two right-handed helices in the 2x2 supercell, and each has four counter-rotating and two co-rotating neighbours. Energy minimization shows that it is impossible to have $\alpha = \pi/2$ for all rows simultaneously; instead the best solution has $\alpha = \pi/2$ for co-rotating and $\alpha = \frac{5\pi}{12}$ for counter-rotating columns (Fig. 4k1), with interaction energy per dimer about –45.6 (Table S11). Co-rotating columns having $\alpha = \pi/2$ means that neighbouring helices are vertically shifted by quarter-pitch (Fig. 4i). This results in a 3D

orthorhombic cell with *Fddd* symmetry, fitting almost exactly our observed dimer orientations at different elevations (*cf.* Figs. 4k1 and 4b/3.5Å).

Other possible arrangements of helical columns have also been explored (Figs. 4k2-4k4). The energies for models 1-4 were -45.6, -36.75, 15 and 15 respectively. The energy of Model 1, our proposed *Fddd* structure, was clearly the lowest. In comparison, the calculated energy for a completely uncorrelated Col phase is 18. For more details see Section S9, SI. It is therefore concluded that the *Fddd* structure is a result of packing optimization of helical columns with non-circular cross-section.

Spectra and π-π stacking

With conjugated fluorophore cores, **FCN16** and **FO16** are potential electroptic materials[36,37]. Their UV-vis and fluorescence spectra are shown in Fig. 5 together with HOMO and LUMO orbitals calculated by density functional theory (DFT). The bandgaps measured from **FO16** and **FCN16** spectra in Col phase are 2.15 and 1.52 eV, smaller than calculated (Fig. 5 and Table S10) due, at least partly, to the neglect of intermolecular conjugation in the calculation. The bandgaps narrowed by a further 0.07 and 0.17 eV on Col-*Fddd* transition, causing red shifts of ~20 and 50-60 nm in **FO16** and **FCN16**. These results indicate an increase in intermolecular conjugation upon the transition. In the Col phase 4.5Å thick three-molecule strata orient randomly in the *xy* plane (Figs. 2f, S13a, 3l,m). On Col-*Fddd* transition the number of molecules drops to two and the inter-strata spacing to 3.5Å. The particularly large bandgap narrowing in **FCN16** is consistent with the potent malononitrile acceptor (Hammett constant for CN σ_p=0.66[38]) interacting strongly with electron-rich adjacent aromatic cores[39] and stabilizing the π-stack[40]. **FCN16** stands out also by its large transition enthalpy (17J/g) and increase in birefringence (Fig. 1c,d). The near-IR fluorescence, expected in FCN16, could be useful in achieving greater light penetration through opaque tissue[41].

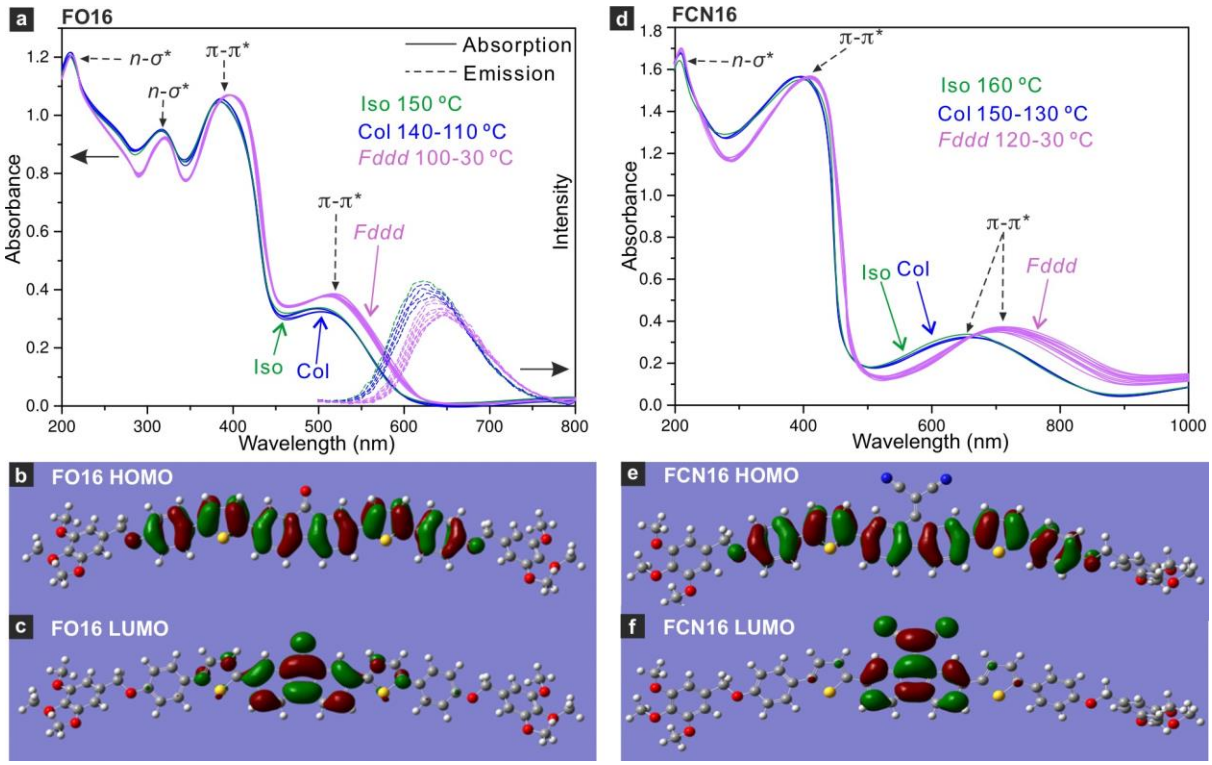

Fig. 5 UV-vis-fluorescence spectra and HOMO-LUMO orbitals. a, UV-vis and fluorescence emission spectra and **b** HOMO and **c** LUMO orbital isosurfaces of **FO16**. **d**, UV-vis, **e** HOMO and **f** LUMO orbitals of **FCN16**. Spectra are recorded during cooling from isotropic phase. **FO16** emission is excited at 420 nm. HOMO and LUMO energies and bandgaps calculated by DFT (B3LYP/6-31G) are E_{HOMO} = -5.02 eV, E_{LUMO} = -2.25 eV, ΔE = 2.77 eV for **FO16** and E_{HOMO} = -5.11 eV, E_{LUMO} = -3.12 eV, ΔE = 1.99 eV for **FCN16**. The bandgaps measured from vis spectra by the Tauc plot method[42] are 2.15 eV (Col) and 2.10 eV (*Fddd*) for **FO16,** and 1.52 eV (Col) and 1.35 eV (*Fddd*) for **FCN16** (see Table S10). **FCN16** is expected to emit in near IR (not measured).

Conclusions

In summary, a new complex 3D liquid-crystal phase is discovered in bent- and straight-core compounds, having orthorhombic *Fddd* symmetry and consisting of counter-rotating helical columns. Unlike previous reports of helical columnar LCs, in spite of being non-crystalline, helical periodicity is long-range and spontaneous. As antichiral near-neighbour interactions are favoured, the structure is equivalent to an antiferromagnet, hence termed antiferrochiral. Its discovery confirms the universality of the principle of twisting polycatenar columns as building blocks for complex 3D self-assembly, previously established in bicontinuous LCs, albeit here without network junctions. The long-range twist sense is shown to propagate through mere steric inter-helical interaction. Comparison of different helical packing models based on linear quadrupoles confirms that *Fddd* is the lowest energy solution.

Other helical column phases could be designed on similar principles. E.g. a spontaneously chiral phase with one[30] (Fig. 4k3) or 3 helices per cell may be devised, where chiralities could not cancel; the latter exists e.g. in β-form of crystalline *i*-polypropylene[43]. With suitable fluorophores this could lead to new organic circularly-polarized LEDs, enantioselective filters or sol-gel templates for ceramics.

References

1. Oswald P. & Pieranski P. *Smectic and Columnar Liquid Crystals: Concepts and Physical Properties Illustrated by Experiments* (CRC Press, Boca Raton, 2005).
2. Sun H. J., Zhang S. D. & Percec V. From structure to function via complex supramolecular dendrimer systems. *Chem. Soc. Rev.* **44**, 3900-3923 (2015).
3. Vera F., Serrano J. L. & Sierra T. Twists in mesomorphic columnar supramolecular assemblies. *Chem. Soc. Rev.* **38**, 781-796 (2009).
4. Wohrle T. *et al.* Discotic Liquid Crystals. *Chem. Rev.* **116**, 1139-1241 (2016).
5. Kato T., Yasuda T., Kamikawa Y. & Yoshio M. Self-assembly of functional columnar liquid crystals. *Chem. Commun.*, 729-739 (2009).
6. Fall W. S. *et al.* Molecular ejection transition in liquid crystal columns self-assembled from wedge-shaped minidendrons. *Soft Matter* **15**, 22-29 (2019).
7. Li Y. X. *et al.* New Type of Columnar Liquid Crystal Superlattice in Double-Taper Ionic Minidendrons. *Chem. Eur. J.* **25**, 13739-13747 (2019).
8. Cheng X. *et al.* Calamitic bolaamphiphiles with (semi) perfluorinated lateral chains: polyphilic block molecules with new liquid crystalline phase structures. *J. Am. Chem. Soc.* **125**, 10977-10996 (2003).
9. Chen B. *et al.* Liquid crystalline networks composed of pentagonal, square, and triangular cylinders. *Science* **307**, 96-99 (2005).
10. Ungar G. *et al.* Self-Assembly at Different Length Scales: Polyphilic Star-Branched Liquid Crystals and Miktoarm Star Copolymers. *Adv. Funct. Mater.* **21**, 1296-1323 (2011)
11. Destrade C. *et al.* Disc-like Mesogen Polymorphism. *Mol. Cryst. Liq. Cryst.* **106**, 121-146 (1984).
12. Gharbi M., Gharbi A., Nguyen H. T. & Malthete J. Polycatenar liquid crystals with long rigid aromatic cores: a review of recent works. *Curr. Opin. Colloid Interface Sci.* **7**, 312-325 (2002).
13. Fontes E., Heiney P. A. & de Jeu W. H. Liquid-Crystalline and Helical Order In a Discotic Mesophase. *Phys. Rev. Lett.* **61**, 1202-1205 (1988).
14. Metzroth T. *et al.* Unravelling the fine structure of stacked bipyridine diamine-derived C3-discotics as determined by X-ray diffraction, quantum-chemical calculations, Fast-MAS NMR and CD spectroscopy. *Chem. Sci.* **2**, 69-76 (2011).
15. Zagrovic B. Helical signature motif in the fibre diffraction patterns of random-walk chains. *Mol. Phys.* **105**, 1299-1306 (2007).
16. Baumgarten J. L. Ferrochirality: a simple theoretical model of interacting, dynamically invertible, helical polymers, 2. Molecular field approach: supports and the details. *Macromol. Theory Simul.* **4**, 1-43 (1995).
17. Kutsumizu S. Recent Progress in the Synthesis and Structural Clarification of Thermotropic Cubic Phases. *Isr. J. Chem.* **52**, 844-853 (2012).
18. Zeng X. B., Ungar G. & Imperor-Clerc M. A triple-network tricontinuous cubic liquid crystal. *Nat. Mater.* **4**, 562-567 (2005).
19. Dressel C. *et al.* Dynamic mirror-symmetry breaking in bicontinuous cubic phases. *Angew. Chem. Int. Ed.* **53**, 13115-13120 (2014).
20. Zeng X. B. & Ungar G. Spontaneously chiral cubic liquid crystal: three interpenetrating networks with a twist. *J. Mater. Chem. C*, 5389-5398 (2020)

21. Lu H. J. *et al.* The Solution of the Puzzle of Smectic-Q: The Phase Structure and the Origin of Spontaneous Chirality. *Angew. Chem. Int. Ed.* **57**, 2835-2840 (2018).
22. Wang L. *et al.* Extraordinary Acceleration of Cogwheel Helical Self-Organization of Dendronized Perylene Bisimides by the Dendron Sequence Encoding Their Tertiary Structure. *J. Am. Chem. Soc.* **142**, 9525-9536 (2020).
23. Heiney P. A., Fontes E., de Jeu W. H., Riera A., Carroll P. & . Smith, A. B. Frustration and helicity in the ordered phases of a discotic compound. *J. Physique* **50**, 461-483 (1989).
24. Clark E. S. & Muus L. T. Partial disordering and crystal transitions in polytetrafluoroethylene. *Z. Kristallogr.* **117**, 119-127 (1962).
25. Ungar G. Thermotropic hexagonal phases in polymers: common features and classification. *Polymer* **34**, 2050-2059 (1993).
26. Savin A. V. & Manevitch L. I. Topological solitons in spiral polymeric macromolecules: A chain surrounded by immovable neighbors. *Phys. Rev. B* **63**, 224303 (2001).
27. Cheng H. F. *et al.* Trigonal columnar self-assembly of bent phasmid mesogens. *Chem. Commun.* **54**, 156-159 (2018).
28. Kleman M. Developable domains in hexagonal liquid-crystals. *J. Phys*ique **41**, 737-745 (1980).
29. In lyotropic surfactant a distinction is made between helical ribbons (wound-up tapes with non-zero mean curvature, precursor of helical tubes) and twisted ribbons (only Gaussian, or saddle curvature). The ribbons referred to in the current paper are of the latter type, even though the term “helical” is often used. See Oda R. *et al.* Tuning bilayer twist using chiral counterions. *Nature* **399**, 566-569 (1999).
30. Shcherbina M. A. *et al.* Hollow Six-Stranded Helical Columns of a Helicene. *Angew. Chem. Int. Ed.* **48**, 7837-7840 (2009).
31. Takezoe H. Polar liquid crystals – ferro, antiferro, banana, and columnar. *Mol. Cryst. Liq. Cryst.* 646, 46-65 (2017).
32. Meuler A. J., Hillmyer M. A. & Bates F. S. Ordered Network Mesostructures in Block Polymer Materials. *Macromolecules* **42**, 7221-7250 (2009).
33. Tyler C. A. & Morse D. C. Orthorhombic Fddd network in triblock and diblock copolymer melts. *Phys. Rev. Lett.* **94**, 208-302 (2005).
34. *a* is defined as the largest lattice parameter as used in this paper, and in the following parameters from literature have been changed accordingly for easier comparison.
35. Wang X.-B., Lo T.-Y., Hsueh H.-Y. & Ho R.-M. Double and Single Network Phases in Polystyrene-block-poly(l-lactide) Diblock Copolymers. *Macromolecules* **46**, 2997-3004, (2013).
36. Chakraborty C. *et al.* Vice versa donor acceptor fluorene–ferrocene alternate copolymer: a twisted ribbon for electrical switching. *Chem. Commun.* 51, 13123-13126 (2015).
37. Kim D. *et al.* Solution-processable fluorene derivative for organic thin-film transistors. *Org. Electron.* **76**, 105464, (2020).
38. http://www.wiredchemist.com/data/hammett-sigma-constants
39. Hansch C., Leo A. & Taft R. W. A survey of Hammett substituent constants and resonance and field parameters. *Chem. Rev.* **91**, 165-195 (1991).
40. Nuckolls C. *et al.* Synthesis and Aggregation of a Conjugated Helical Molecule. *J. Am. Chem. Soc.* **121**, 79-88 (1999).
41. Ravetz B. D. *et al.* Photoredox catalysis using infrared light via triplet fusion upconversion. *Nature* **565**, 343-346, (2019).
42. Tauc J., Grigorovici R. & Vancu A. Optical Properties and Electronic Structure of Amorphous Germanium. *Phys. Stat. Solidi (b)* **15**, 627-637 (1966).
43. Meille S. V. *et al.* Structure of β-Isotactic Polypropylene: A Long-Standing Structural Puzzle. *Macromolecules* **27**, 2615-2622 (1994).

Methods

Synthesis. The synthesis of bent compounds **IC^3/n** (n=10, 12 and 14) have been reported previously[27]. Synthesis and chemical characterization of the straight-core compounds **FO16** and **FCN16** is described in Section S10 in SI.

Transmission powder SAXS/WAXS experiments were carried out at station I22 of Diamond Light Source, U.K. Powder samples in 1 mm glass capillaries were held in a modified Linkam hot stage. Pilatus 2M detector (Dectris) was used and the X-ray energy was 12.4 keV. GISAXS/GIWAXS experiments were done at BM28 of European Synchrotron Radiation Facility, France, and I16 of Diamond Light Source. 2d diffraction patterns were collected using a MAR165 CCD camera at BM28 and Pilatus 2M at I16. Thin film samples were prepared from melt on silicon substrate. *n*-tetracontane was used to calibrate the sample to detector distance.

Electron density maps were calculated by inverse Fourier transformation using standard procedure as described in International Tables for Crystallography. Integral intensities of all peaks were measured using Gaussian peak fitting. GISAXS intensities were used to help resolve overlapping peaks. More details are in SI.

Molecular models were built using Materials Studio (Accelrys). Geometry optimization and molecular dynamic annealing were performed using Forcite Plus module with Universal Force Field. NVT annealing dynamics was performed through 30 cycles between 300 and 600 K, with a total annealing time of 30 ps. Frontier orbital distributions of fluorene derivatives were calculated using the DFT at level B3LYP, 6-31G(d) basis set.

AFM imaging was done in tapping mode on a Bruker Multimode 8 instrument with Nanoscope V controller. The sample was dissolved in toluene and spin-coated on a highly ordered pyrolytic graphite substrate.

For UV-vis and fluorescence emission spectroscopy the samples were melted and spread evenly between quartz plates (1 mm thickness). UV-vis spectra were recorded using Lambda 900 (Perkin Elmer). Fluorescence spectra of **FO16** were excited at 420 nm and recorded by Fluoromax4 (Horiba).

DSC thermograms were recorded on a DSC 200 F3 Maia calorimeter (NETZSCH) with heating/cooling rates as specified.

Polarized optical micrographs were recorded using an Olympus BX-50 equipped with a Mettler HS82 hot stage.

Acknowledgements

For support with experiments at Diamond Light Source we thank Dr Olga Shebanova and Prof. Nick Terill (I22) and Dr Gareth Nisbet and Prof. Steve Collins (I16), as well as Drs Oier Bikondoa and Paul Thompson at XMaS beamline (BM28) at ESRF. We also thank Prof. Julia Weinstein for help with fluorescence spectroscopy. Financial support is acknowledged from the 111 Project 2.0 of China (BP2018008), from EPSRC (EP-P002250, EP-T003294), from NSFC (21865038) and Yunnan Joint Fund Key Project (2018FY001(-012)). YXL thanks CSC for stipend and UoS for fee waiver.

Author Contributions

XHC, XBZ and GU supervised the study. HFG and QC synthesised and characterized the compounds chemically, HFG performed DFT calculations. YXL carried out X-ray, UV-vis, fluorescence experiments, reconstructed ED maps and performed MD simulation. RBZ and YXL performed AFM experiments. KG, GAG and XBZ developed the packing theory for helices. GU, XBZ and YXL wrote the paper with contributions from all authors. All authors discussed the results and commented on the manuscript.

Competing Interests

The authors declare no competing financial interest.

Additional information

Supplementary information, including videos, is available at

Table of Contents Picture

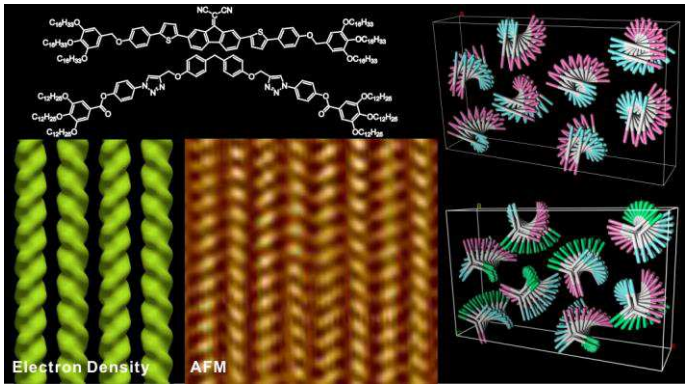

Figures

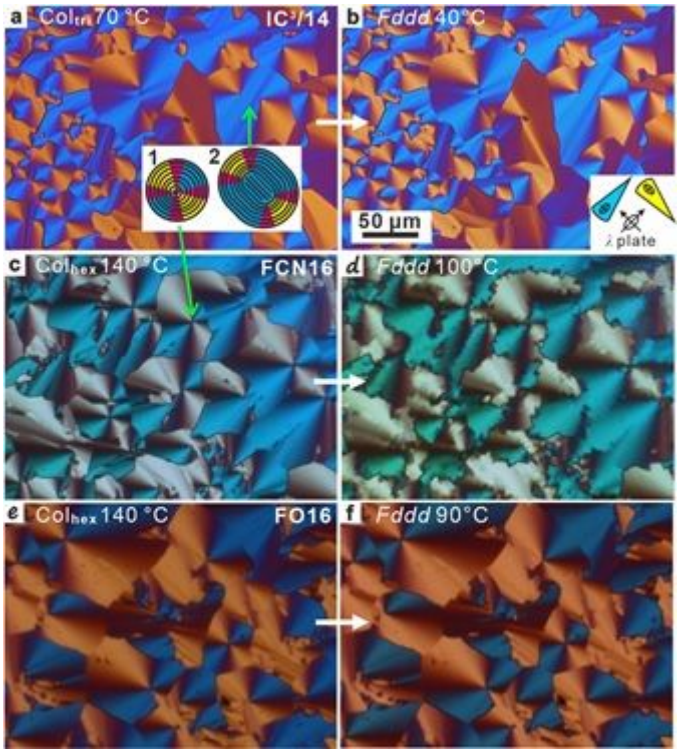

Figure 1

Polarized optical micrographs. a,c,e, columnar and b,d,f, Fddd phases of compounds (a, b) IC3/14, (c, d) FCN16 and (e, f) FO16. Recorded with a full-wave (λ) plate. Inset in a depicts two developable domains with (1) a s=+1 disclination and (2) two +½ disclinations, the latter indicating stiffer columns; black lines are column trajectories. Inset in b shows orientation of indicatrices of λ-plate and coloured fans. See more textures in Section S2, SI.

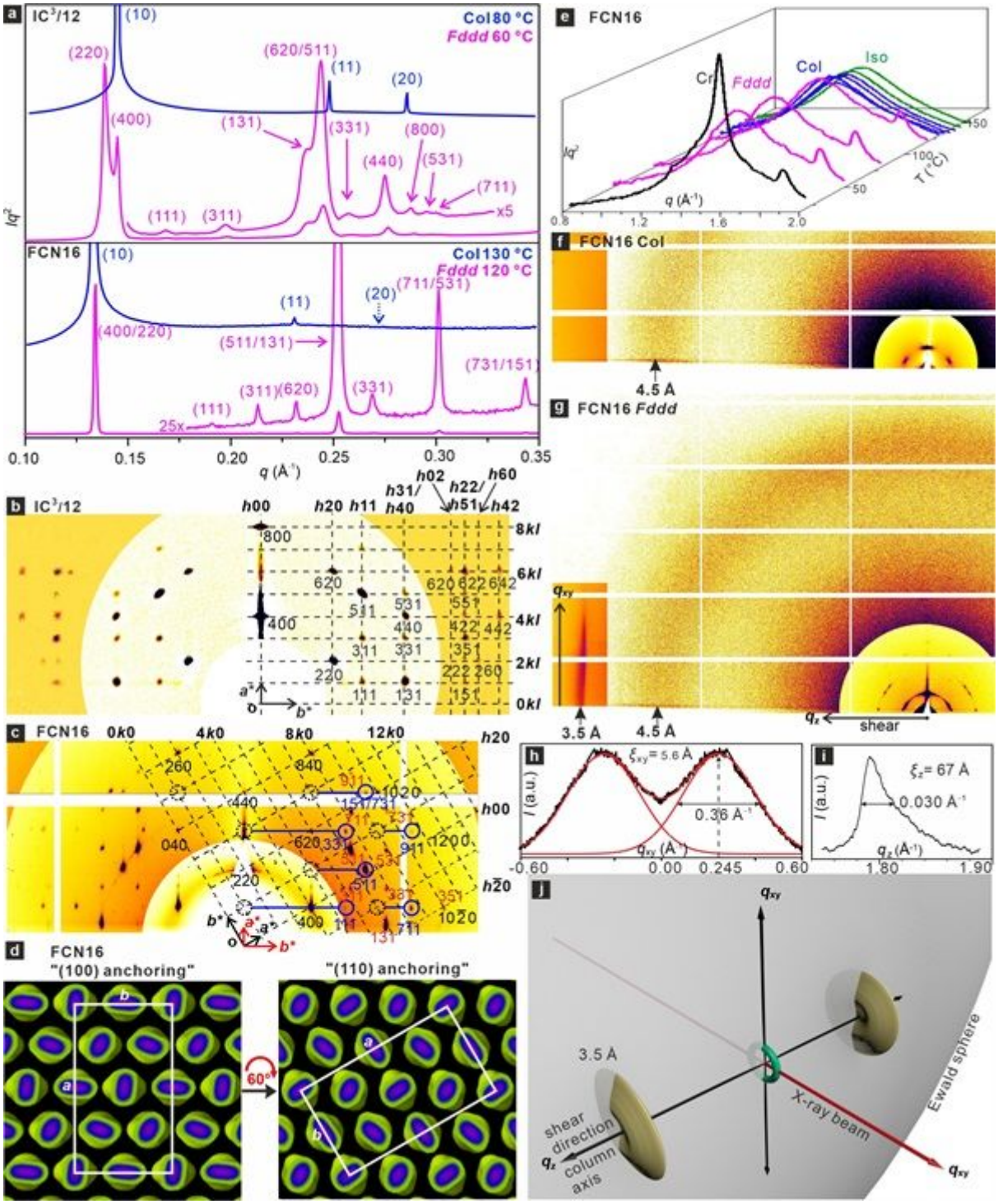

Figure 2

X-ray diffraction results. a, Transmission powder SAXS curves of Col and Fddd phases of IC3/12 and FCN16. b,c, GISAXS patterns of Fddd phase of IC3/12 and FCN16. Background was subtracted and the higher-q zone is intensity-enhanced. Partial reciprocal hk0 lattice plane is superimposed, with some hkl spots in c circled blue and con-nected to their hk0 base by blue row lines (for calculation see Fig. S9). Reflections in c come from two orientations with (110) and (100) planes anchored on Si substrate; reflections in red are from the latter. d, Real space FCN16: in both orientations the LC faces substrate with a dense plane of columns (unit cell in white). e, Evolution of powder WAXS of FCN16 on heating. f,g,

GIWAXS of lightly sheared film of FCN16 in Col (130°C) and Fddd (100°C) phases, respectively; note the absence of the 3.5Å streak in Col. h,i, qxy (vertical) and qz (hori-zontal) scans of the 3.5Å streak in g; in h the peak is reflected across the horizon to facilitate curve resolution. j, Reciprocal space descrip-tion of diffraction geometry in g, showing symbolically a SAXS ring and the 3.5Å disks.

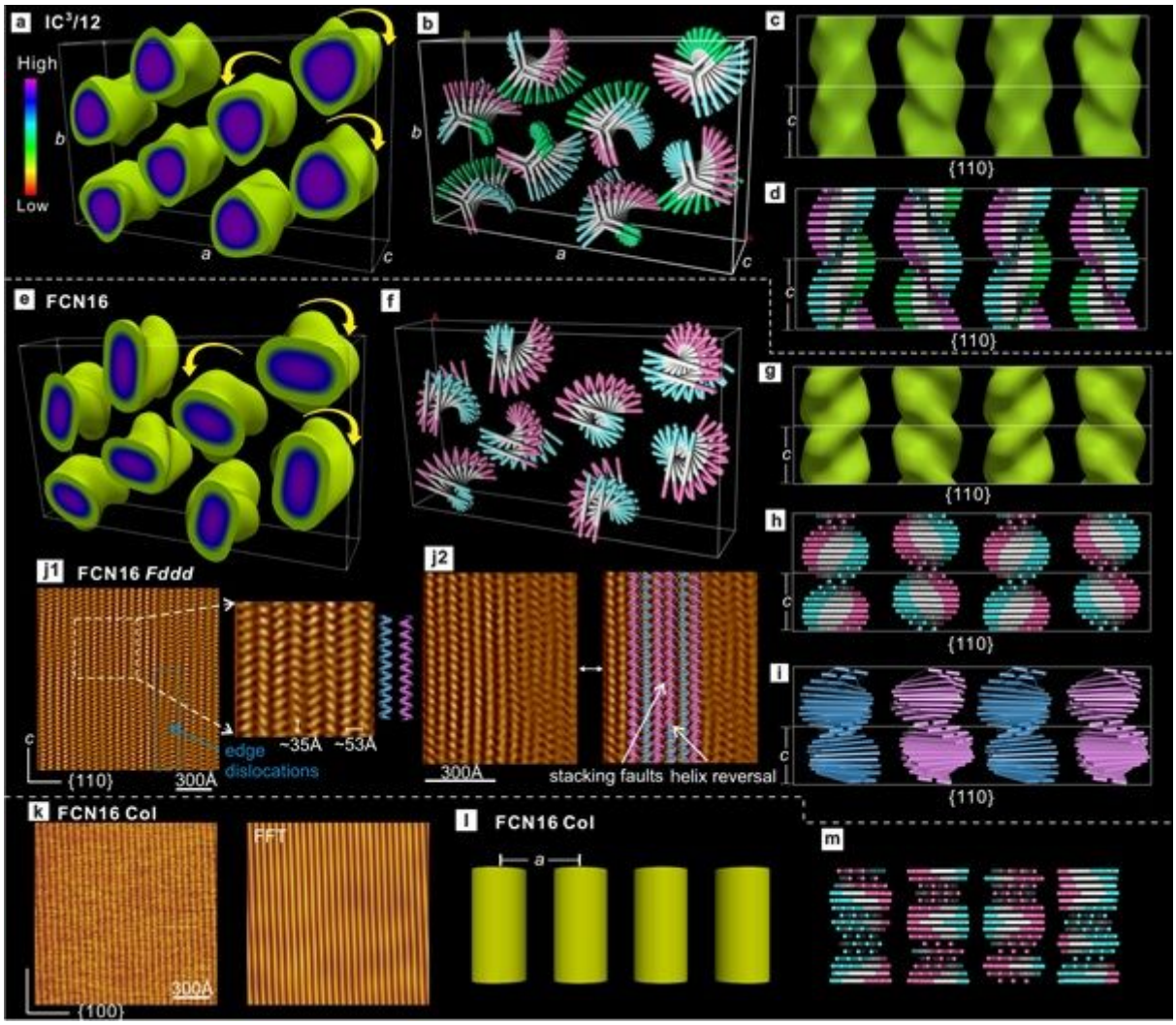

Figure 3

ED maps, schematic models and AFM images. ED maps and stylized models of Fddd phase of (a-d) IC3/12 and (e-h) FCN16, and (l,m) of the Col phase of FCN16. (a,c,e,g) 3D maps with high ED regions (aromatic) enclosed within isoelectron surface (see also supporting videos). (b,d,f,h), Schematic models of winding rod-like molecular cores (“staircases”. The two or three core end-groups are coloured differently for clarity. The high positional order is grossly exaggerated. c,d,g,h, View along b-axis. i. A more realistic model of h taking account of the 8° molecular tilt. j, AFM of Fddd phase of FCN16 recorded at 50 °C (Fourier-filtered height image). The enlarged area shows alternating left- and right-handed columns; stacking faults of mismatched chirality and a helix reversal are indicated in (j2). k, original AFM image and inverse FFT of Col phase of FCN16. l, ED map (time/space average by SAXS) and m, random twist model (an instantaneous arrangement) of Col phase of FCN16.

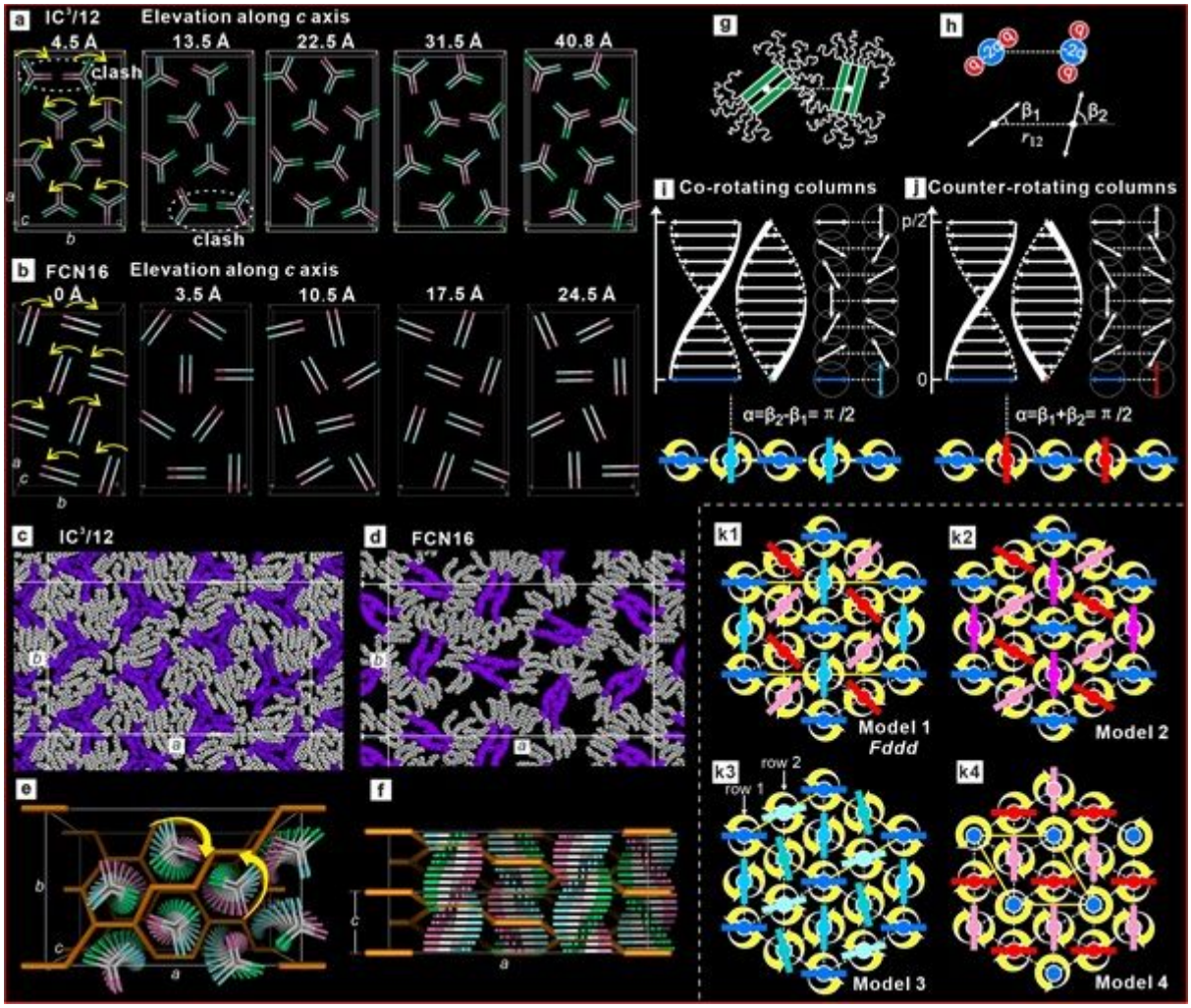

Figure 4

Models of Fddd and its alternatives. a,b, Layers at different z-elevation for (a) IC3/n and (b) FCN16/FO16. c,d, Snapshots of MD-annealed atomistic models (xy layer; purple: aromatic, grey/white: aliphatic). e,f, Comparison of network model of Fddd phase in poly(styrene-b-isoprene) (yellow rods) with model of IC3/n. Arrows indicate helical sense of both columns and network. g,h, Two dimers of FO16/FCN16 on neighbouring columns in g represented by quadrupoles in h, where geometrical parameters are also defined. i,j, Side and top views of (i) co-rotating and (j) counter-rotating ribbons. k. Minimum energy configurations on a 2D hexagonal lattice; (k1) two left- and two right-handed columns in a 2x2 supercell, equivalent to the Fddd structure here observed experimentally; (k2) three left- and one right-handed column in a 2x2 supercell; (k3) four right-handed columns in a 2x2 supercell; it turns out that vertical shifting of the second row of columns relative to the first does not change the system energy (k4) two left- and one right-handed column in a supercell. The orientation of right-handed columns can be random, which does not affect the system energy (cf. structure in ref. 23). In (k1-k4) right- (left-)handed columns are shades of blue (red).

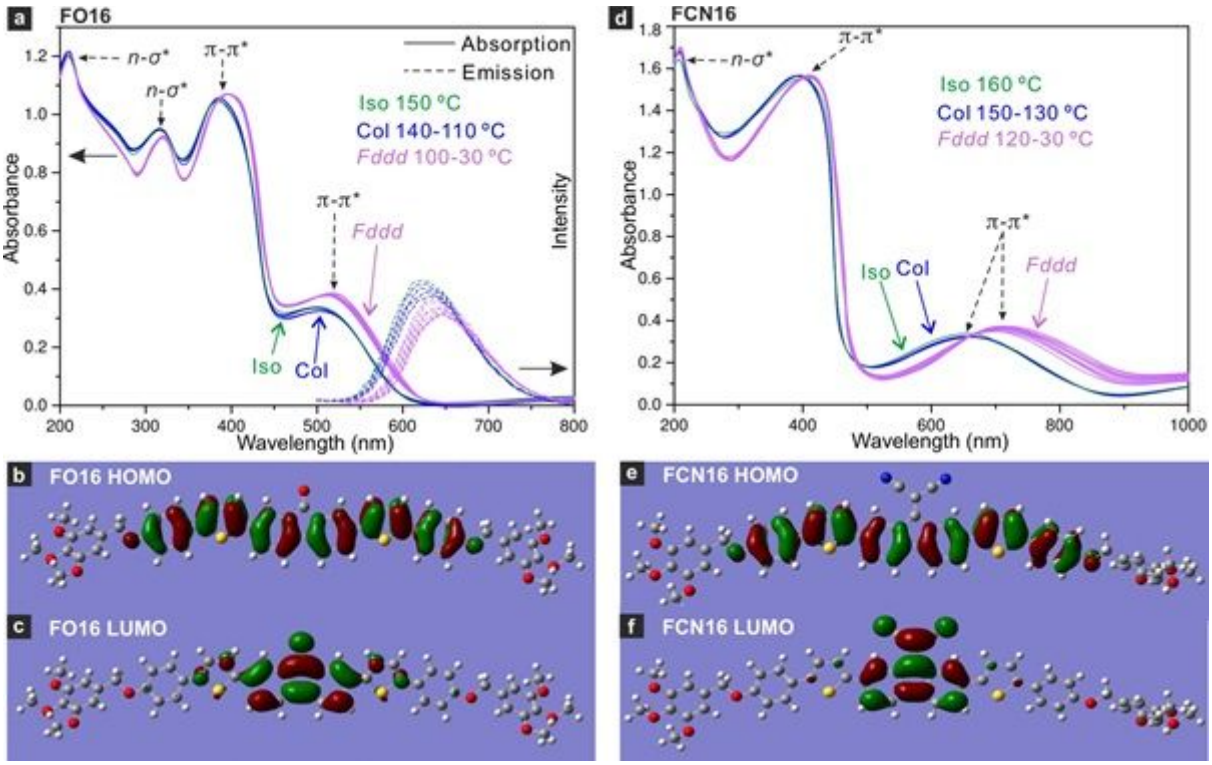

Figure 5

UV-vis-fluorescence spectra and HOMO-LUMO orbitals. a, UV-vis and fluorescence emission spectra and b HOMO and c LUMO orbital isosurfaces of FO16. d, UV-vis, e HOMO and f LUMO orbitals of FCN16. Spectra are recorded during cooling from isotropic phase. FO16 emission is excited at 420 nm. HOMO and LUMO energies and bandgaps calculated by DFT (B3LYP/6-31G) are EHOMO = -5.02 eV, ELUMO = -2.25 eV, DE = 2.77 eV for FO16 and EHOMO = -5.11 eV, ELUMO = -3.12 eV, DE = 1.99 eV for FCN16. The bandgaps measured from vis spectra by the Tauc plot method are 2.15 eV (Col) and 2.10 eV (Fddd) for FO16, and 1.52 eV (Col) and 1.35 eV (Fddd) for FCN16 (see Table S10). FCN16 is expected to emit in near IR (not measured).

Supplementary Files

This is a list of supplementary files associated with this preprint. Click to download.

- YXLietal320x240videos.rar
- YXLietalSI.pdf
- GraphicalAbstract.jpg